Journal of Instrumentation

Design and test of μSR detection system of EMuS at CSNS

To cite this article: X.J. Ni *et al* 2019 *JINST* **14** T04004

View the article online for updates and enhancements.

IOP ebooks™

Bringing you innovative digital publishing with leading voices to create your essential collection of books in STEM research.

Start exploring the collection - download the first chapter of every title for free.

This content was downloaded from IP address 211.86.148.153 on 09/04/2019 at 11:40

Published by IOP Publishing for Sissa Medialab

Received: *January 30, 2019*
Accepted: *March 31, 2019*
Published: *April 8, 2019*

TECHNICAL REPORT

Design and test of μSR detection system of EMuS at CSNS

X.J. Ni,[a,1] **Z.W. Pan,**[a,1] **F.S. Deng,**[a] **M.Q. Zhuang,**[a] **Y.G. Zhang,**[a] **J.Y. Dong,**[a] **H. Liang,**[a] **J.Y. Tang**[b] **and B.J. Ye,**[a,2]

[a] *State Key Laboratory of Particle Detection and Electronics, University of Science and Technology of China, Hefei 230026, China*

[b] *Institute of High Energy Physics, Chinese Academy of Sciences, Beijing 100049, China*

E-mail: bjye@ustc.edu.cn

Abstract: EMuS (Experimental Muon Source) as the first muon source in China will be built at China Spallation Neutron Source (CSNS). A 128-channel μSR spectrometer prototype is under development for EMuS. As the core part of μSR spectrometer prototype, the detection system (detectors and readout electronics) has been constructed. Beam test (at ISIS Muon Source in U.K.) and magnetic shielding test have been carried out to test the performances of this detection system. In this paper, a new test method has been developed to test the magnetic shielding capability by using the energy spectrum of ^{22}Na source. A magnetic field up to at least 30 Gauss can be eliminated by the proposed shielding. This satisfies the actual requirement of 8 Gauss. The dead time of the prototype detector was measured with a dedicated setup and measured to be 1.4 ns.

Keywords: Data acquisition circuits; Detector design and construction technologies and materials; Muon spectrometers; Large detector-systems performance

[1]These authors contributed equally to this work.
[2]Corresponding author.

© 2019 IOP Publishing Ltd and Sissa Medialab
https://doi.org/10.1088/1748-0221/14/04/T04004

2019 JINST 14 T04004

Contents

2019 JINST 14 T04004

1 Introduction

μSR (muon spin relaxation, rotation, and resonance) has become an important technology to study the atomic-level chemical and physical properties of condensed matter since the 1980s [1, 2]. Those techniques have been usually used to study magnetic materials, superconductors, ions transport, semiconductors, chemistry, and biological materials [3–7]. Due to the high polarizability (close to 100% for surface muons) of the muons produced by an accelerator, μSR is especially suitable for studying the magnetism of condensed matter.

μSR spectrometers are mainly located in four accelerator facilities (ISIS/U.K., PSI/Switzerland, J-PARC/Japan, and TRIUMF/Canada) [8–11]. The muon beams for μSR applications in these facilities are classified into DC muon beams (PSI and TRIUMF) and pulsed muon beams (ISIS and J-PARC) according to their different time structures. The great advantage of DC muon beam is that its μSR spectrometers can get an excellent time resolution (~ 100 ps) which allows detection of larger magnetic fields and faster relaxation signals. In contrast, μSR spectrometers of the pulsed muon beam don't have a good time resolution due to the pulse width of the muon beam. However, for a pulsed muon beam, there is almost no background in μSR signals. That has a great advantage in the detection of muon decay events beyond ten muon lifetimes and measurements of weak spin relaxation [12]. There are other facilities in the progress of developing muon sources (CSNS/China, ROAN/Korea, SNS/America, and RCNP/Japan) [13–16]. China Spallation Neutron Source (CSNS) has been completed in March of 2018. It will provide 5% of the total proton beam power to the EMuS which will be built in the high energy proton experimental area. This makes μSR applications to be realized in China.

μSR spectrometer mainly includes detector arrays, electronics, a sample chamber, and main magnets. The detector arrays usually are made up of plastic scintillators, light guides, and photo-multiplier tubes (PMTs). It can be used to test the time spectrum and asymmetric distribution of the

positrons emitted from the decay of muons in the sample. In this way, the information of the local magnetic field at the muon site in the sample can be obtained. The electronics includes hardware, data acquisition system, control system, running monitoring software, and data processing software. The sample chamber and main magnets can provide different measurement conditions (high temperature, high pressure, extremely low temperature, zero field, longitudinal field, transverse field, and so on). According to users' requirements, there can be different combinations.

Since EMuS is a high-intensity pulsed muon source (repetition rate of 2.5 Hz, pulse width of 50 ns), the instantaneous data rates of muons decay in a pulse are very high. The problem of signal pile-up will be severe which can be solved by increasing the detector segmentation as much as possible. Therefore, a 128-channel μSR spectrometer prototype is under development for EMuS. In this work, we will introduce the integrated design of our μSR spectrometer prototype. Based on the integrated design, the construction of the μSR detection system including detectors and readout electronics have been completed. Since the detectors need to be operated in a strong external magnetic field and the purchased PMTs are very sensitive to the magnetic field, magnetic shielding is essential to the detection system. Therefore, a magnetic shielding case (four layers of 0.1 mm thick permalloy) has been designed and manufactured and a new method to perform the magnetic shielding test based on ^{22}Na energy spectra has been developed. The details are discussed in section 3.1. For a μSR spectrometer based on a pulsed muon source, the dead time of the detection system is a crucial factor which could affect its performance. Section 3.2 reports the details about the beam test performed at ISIS Muon Source in U.K. and the results about the dead time of the detection system.

2 Design and construction of detection system

2.1 Integrated design

As shown in figure 1, the μSR spectrometer prototype is composed of two rings (front and rear). Each ring has 64 channels consisting of plastic scintillators, light guides and PMTs. The covered solid angle, energy threshold of each segment, detection efficiency, collection efficiency, faking event rate, double counting rate, the influence of stray magnetic fields on PMTs, and the influence of a sample chamber and degraders on the asymmetry were carefully considered in the design. After detailed GEANT4 simulations, the parameters of key parts have been confirmed, as shown in figure 1. The planned longitudinal field (LF) of main magnets is in 0–300 Gauss and the transverse field (TF) is tentatively set in 0–100 Gauss. The sample chamber is a closed cycle cryostat. The temperature range is in 10–400 K which can meet basic requirements. A detailed description of the integrated design was reported in our previous paper [17].

2.2 Detector

As shown in figure 1, each detection module is composed of a plastic scintillator (175×13.5×5 mm^3, EJ-200 from Eljen Technology) and a light guide (515.6 × 13.5 × 5 mm^3, Eljen Technology). They were wrapped by Teflon tapes and black tapes, leaving a window to couple with a PMT (Hamamatsu R6427). Figure 2 shows the picture of one detection module of 128-channel μSR spectrometer prototype.

The ratio of signal to noise (SNR), magnetic shielding, and dead time are crucial factors affecting the performances of μSR detectors for a pulsed muon beam. When assembling the μSR

2019 JINST 14 T04004

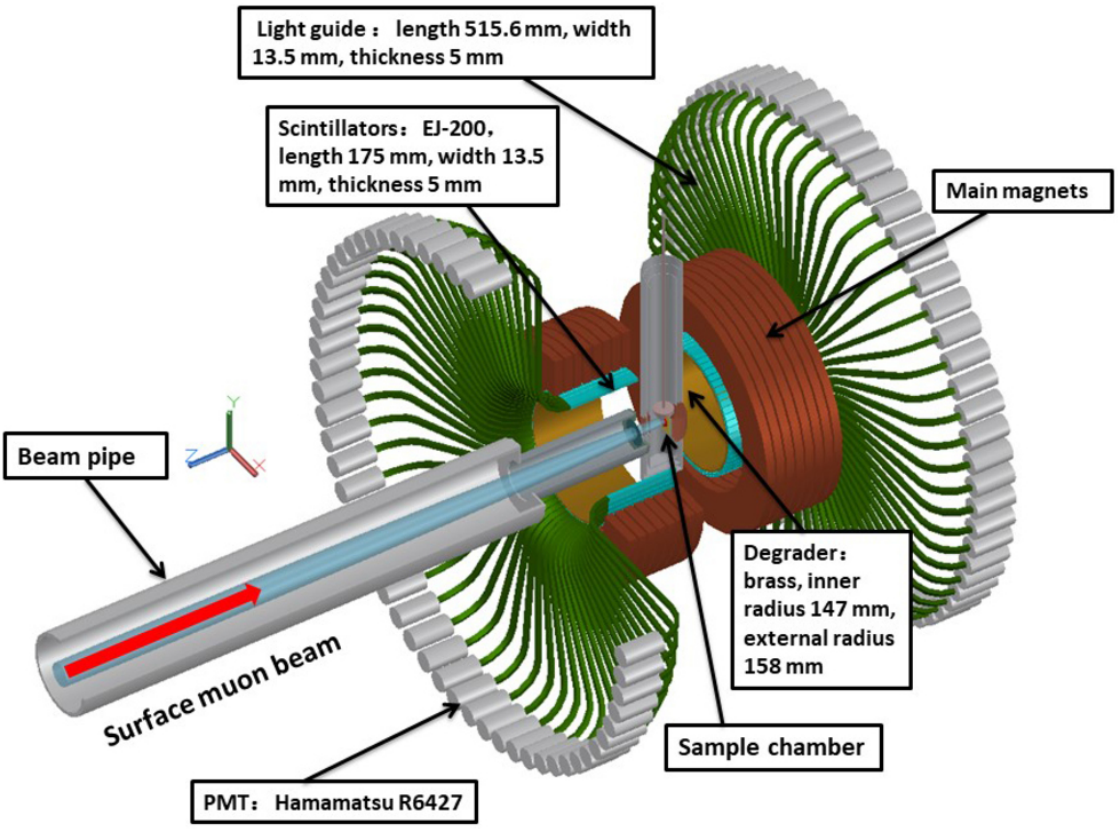

Figure 1. The integrated design of 128-channel μSR spectrometer prototype.

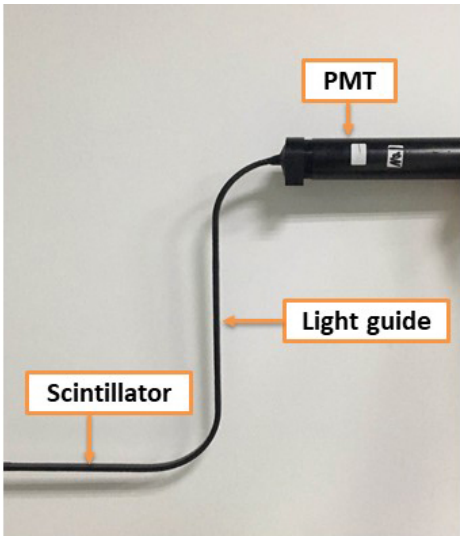

Figure 2. One detection module of 128-channel μSR spectrometer prototype.

2019 JINST 14 T04004

detector, extraneous light should be shielded carefully, otherwise the noise will become very large. The magnetic shielding and beam test will be discussed in detail in section 3.

2.3 Readout and data acquisition

The readout electronics consisting of hardware and data acquisition (DAQ) software has been developed. The hardware includes sixteen 8-channel Front-End Electronics (FEE) and four 32-channel Time-to-Digital Converter (TDC) module [18, 19]. As shown in figure 3, each FEE receives positron signals from eight detectors, and then converts these signals into timing pulses by constant fraction discriminators and hands them to the TDC module as the stop signals. FEE's timing precision is 55 ps [18]. A trigger detector will be set in the upstream of the muon beam to produce a start signal. The TDC module enables 32 channels of time measurement by calculating the time intervals between the start signal and 32-channel stop signals, and then transfers the data to the PC via a Gigabit Ethernet cable. The time resolution of 312.5 ps is achieved by using 16 phase-shifted 200 MHz clocks for data sampling. The core device of the TDC module is a Xilinx Virtex-6 Field Programmable Gate Array (FPGA).

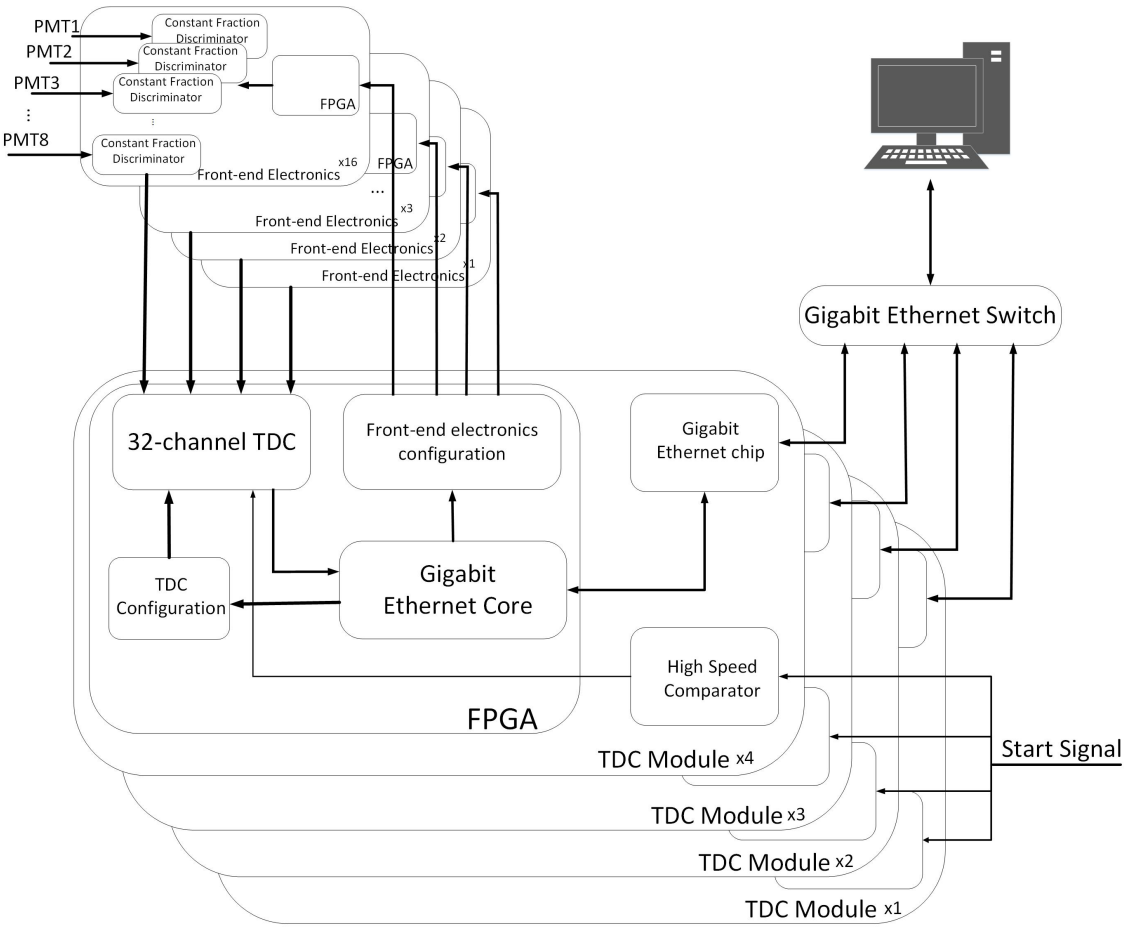

Figure 3. A block diagram of electronics for 128-channel μSR spectrometer prototype.

2019 JINST 14 T04004

The DAQ software can realize the remote configuration of FEEs and TDC modules. Main functions of the DAQ software are listed as follows:

- Self-test: the readout electronics can produce a signal similar to the detector output to detect whether the system can work normally before a real measurement.
- Setting thresholds of FEEs: the background can be suppressed by setting an appropriate threshold.
- Setting the time window of the TDC module: different time measurement ranges can be chosen based on the time structure of the muon beam we used.
- Setting the channel shielding of the TDC module: in an actual situation, some channels may be abnormal or necrosis, so these channels can be shielded selectively.
- Data format conversion: the raw data obtained can be converted to NXS form which can be analyzed by the Mantid software. This software has been widely used in the data analysis of neutron scattering and μSR experiments [20].

A more detailed description of the DAQ architecture and its performances will be reported in our another paper [21].

3 Tests

3.1 Magnetic shielding test

As mentioned above, μSR detectors usually operate in a strong magnetic field. As PMTs are sensitive to the magnetic field, light guides are used to keep them away from the center of the strong magnetic field in the sample area. However, the stray magnetic field can still influence the PMT's performance. Therefore, magnetic shielding is essential to reduce the effect of stray fields.

Firstly, we used G4beamline to optimize the position of PMTs, so that the stray fields at that position can be minimized. Figure 4 shows the magnetic flux density at the optimal position of

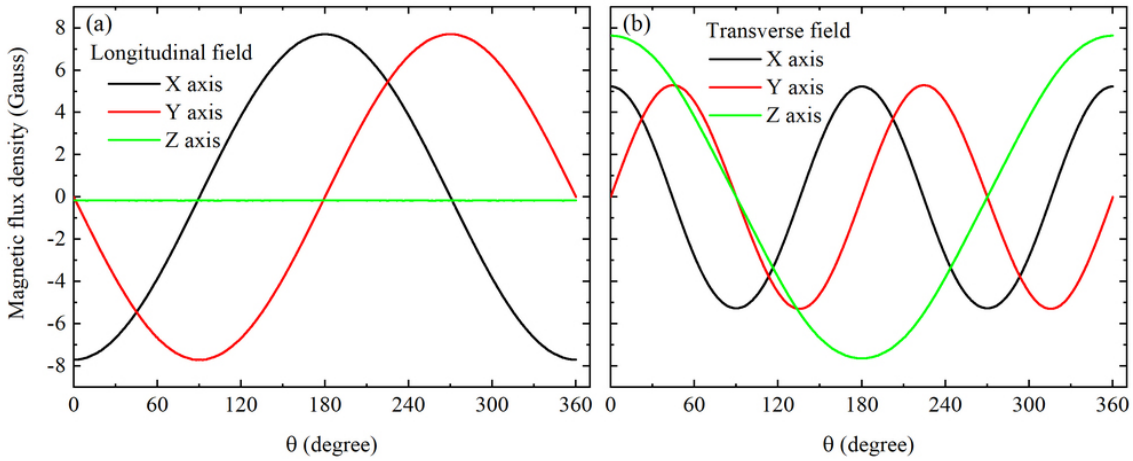

Figure 4. The magnetic flux density at the optimal position of PMTs at LF and TF conditions. θ is the angle between each PMT and the center of the detector ring.

2019 JINST 14 T04004

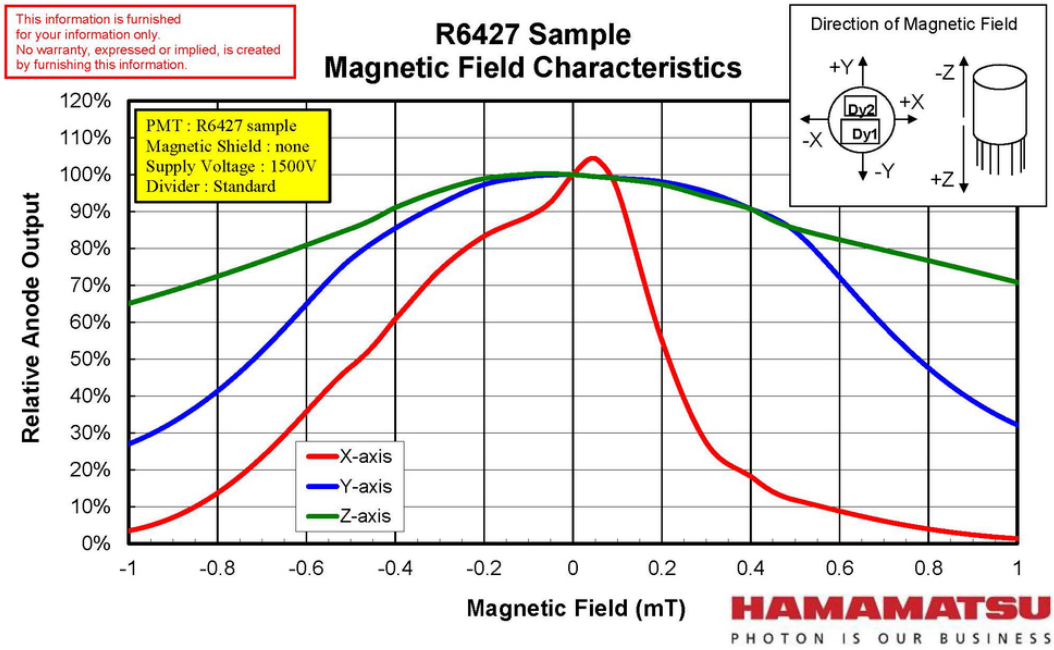

Figure 5. The typical magnetic field characteristics of Hamamatsu R6427 provided by Hamamatsu Photonics K.K.

PMTs at LF and TF conditions (both 300 Gauss). The maximum stray magnetic field is about 8 Gauss which comes from the X/Y (short for X or Y) axis at LF condition and Z axis at TF condition. Figure 5 shows the typical magnetic field characteristics of Hamamatsu R6427 provided by Hamamatsu Photonics K.K. When the magnetic field in the X/Y axis of R6427 is 8 Gauss, the anode output is only about 10–40% left. Therefore, the magnetic shielding for R6427 is very necessary, even though the PMT has been put at an optimal position.

A cylindrical shielding case made up of four layers of permalloy has been designed as mentioned before. Since the region between the photocathode and the first dynode of a PMT is mostly affected by a magnetic field, the photocathode should be positioned deep inside the shielding case by a length longer than or equal to the radius of the shielding case [22]. The radius of our shielding case is designed to 24 mm. The distance between the photocathode and the case edge is 30 mm.

A Helmholtz coil has been made to provide a stable and uniform magnetic field for the test of the magnetic shielding [23]. The diameter of the coils is 300 mm so that the field's homogeneous region ($100 \times 100 \times 100\,\mathrm{mm}^3$) [24] is large enough for the PMT ($\Phi 28.5 \times 85$ mm). The magnetic field range of the Helmholtz coil is 0–65 Gauss. The PMT's magnetic characteristics were tested by measuring ^{22}Na energy spectra. The scintillator we used is LYSO due to its high energy resolution. It was coupled directly to the PMT and a ^{22}Na source was used to generate a signal. They were all put into an insulator (polyflon) covered by the magnetic shielding case. A typical energy spectrum of ^{22}Na has two main energy peaks (0.511 and 1.28 MeV). When the anode out of PMT is influenced by the magnetic field, the energy peak position will change obviously. Capabilities of the magnetic shielding case for the PMT can be measured through this way. Figure 6 shows the magnetic shielding test system.

2019 JINST 14 T04004

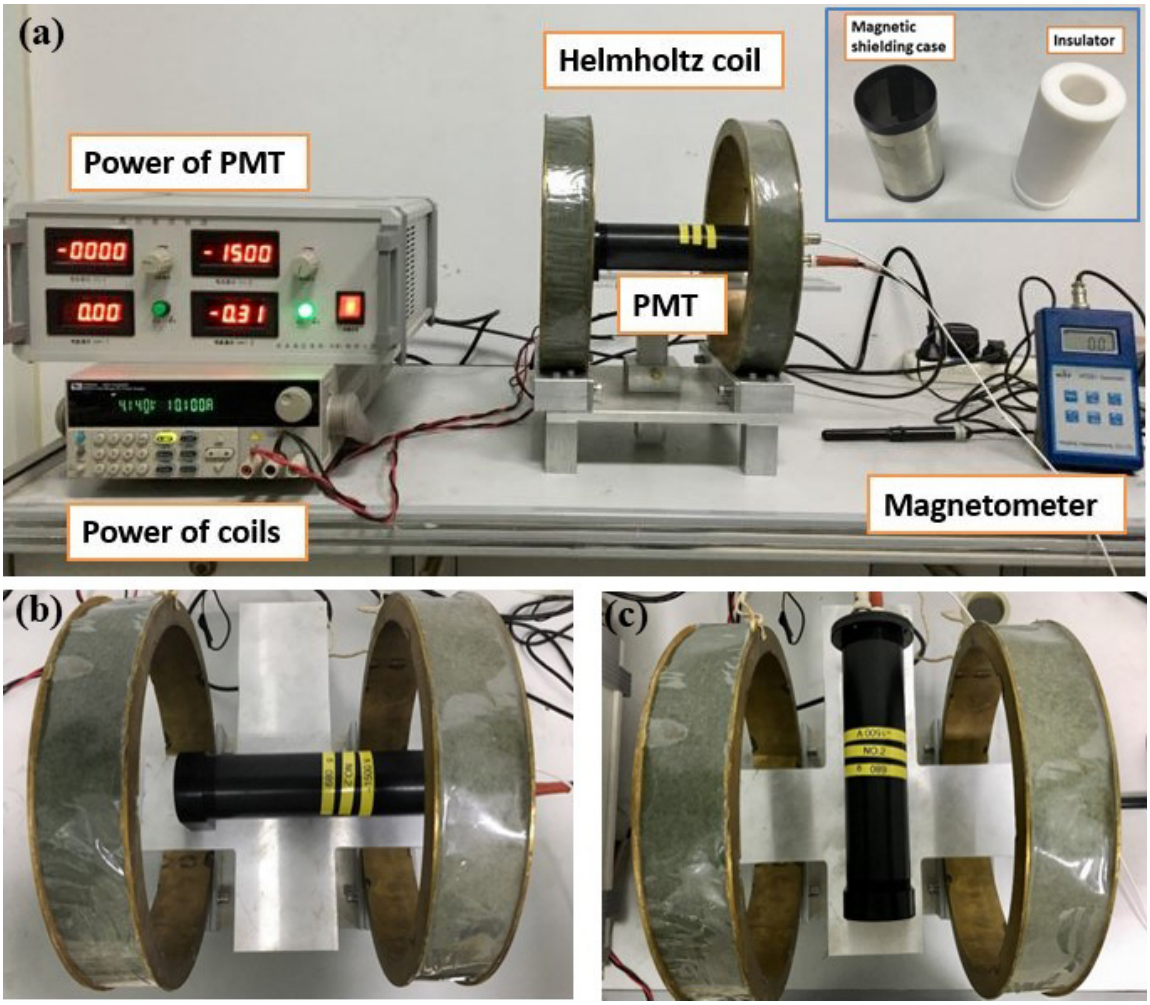

Figure 6. (a) The test system of magnetic shielding. The inset shows the magnetic shielding case and insulator between PMT and case. (b) The magnetic field is parallel to the Z-axis of PMT. (c) The magnetic field is parallel to the X/Y axis of PMT.

Figure 7 (a, b) show the influence of the magnetic field on the PMT parallel or perpendicular to its Z-axis without magnetic shielding. When the magnetic field is absent, the original position of the 0.511 MeV energy peak is at 1677.24 channel. The position of this energy peak moves left by increasing the magnetic field. If the magnetic field is 20 Gauss parallel to the Z-axis or 10 Gauss parallel to the X/Y axis of the PMT, the 0.511 MeV energy peak moves quite obviously. Figure 7 (c, d) show the influence of the magnetic field parallel to the PMT's Z-axis and X/Y axis on the PMT with magnetic shielding. The position of 0.511 MeV energy peak is originally located at 1653.17 channel. When the magnetic field parallel to the Z-axis of PMT is 30 Gauss and parallel to the X/Y axis of PMT is 50 Gauss, the 0.511 MeV energy peak begins to move. It can be concluded that the magnetic shielding is sufficient up to 30 Gauss. This satisfies the actual requirement of 8 Gauss. The same conclusion can be drawn by the change of the total counting rate which is shown in figure 8. There is almost no influence on the total counting rate of ^{22}Na energy spectra when we use the magnetic shielding to the PMT, even though the field is over than 50 Gauss. However,

2019 JINST 14 T04004

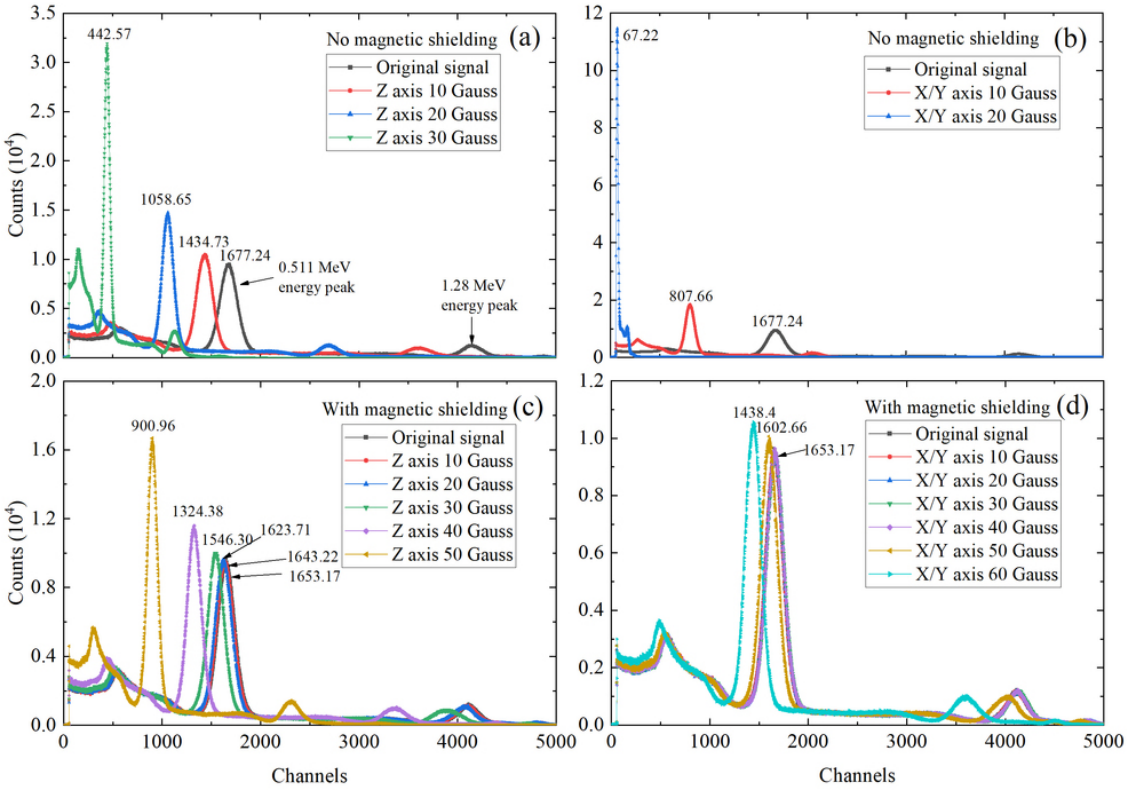

Figure 7. Influence of the magnetic field parallel to the PMT's Z axis and X/Y axis on the PMT (a, b) without magnetic shielding and (c, d) with magnetic shielding. Note that each spectrum was measured in 120 s.

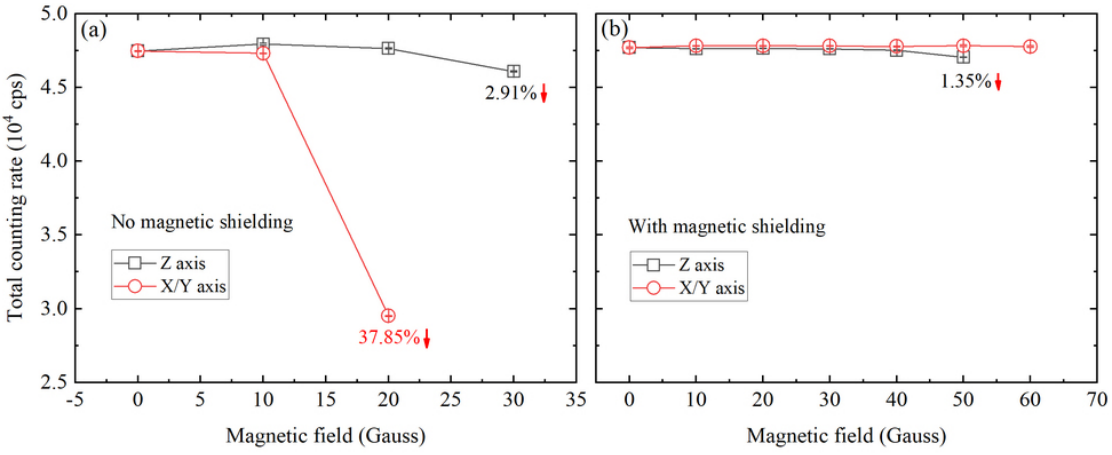

Figure 8. The effect of magnetic fields to the total counting rate of ^{22}Na energy spectra (a) without magnetic shielding and (b) with magnetic shielding.

when the magnetic field parallel to the X/Y axis of PMT is 20 Gauss without magnetic shielding, the total counting rate is decreased by 37.85%. This also means that the PMT is more sensitive to a magnetic field parallel to its X/Y axis.

2019 JINST 14 T04004

3.2 Beam test

Since EMuS is still under development, the detection system was sent to ISIS Muon Group and tested on their muon beam line (assembled on the EMU spectrometer [25]). The ISIS muon source is a pulsed muon source (repetition rate = 40 Hz), it is suitable for our beam test. Silver is used as the test sample and measured in room temperature and zero magnetic field. Figure 9 (a) shows the energy spectrum of positrons emitted from the sample which was detected by our detection system. From this figure, we can see the SNR of our detection system is excellent for signals above 0.15 V amplitude. Figure 9 (b) shows the time spectra of our detector and two EMU detectors with our readout electronics. The time spectrum of decay positrons is crucial for μSR measurements which follows an exponential law: $N(t) = N_0 \exp(-t/\tau_\mu)$ (τ_μ is the muon lifetime of 2.2 μs) [26]. The time spectra measured by both the Chinese detector and the EMU detectors follow the same exponential law. As the size of our scintillator is smaller than that of the EMU detector, the counting rate is lower. The correct energy spectra and time spectra are shown in figure 9 which indicate that the Chinese detector and readout electronics work well.

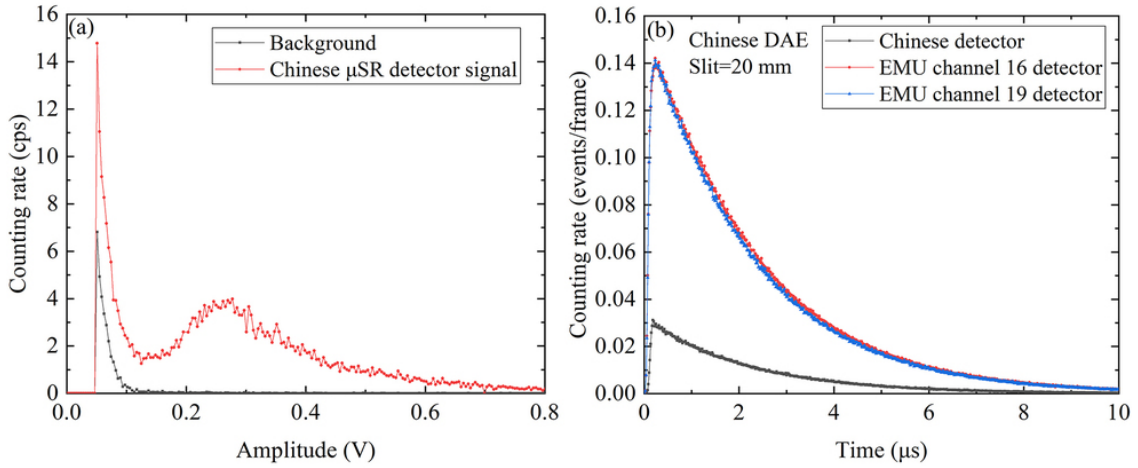

Figure 9. (a) The positron energy spectrum of the detection system. (b) The time spectra of our detector and two EMU detectors. The beam slit is used for tuning beam intensity.

For a pulsed μSR spectrometer, the signal pile-up should be seriously considered, which requires that the dead time of the detection system is as small as possible. Therefore, the dead time test is very important for judging the performance of μSR detection system. In order to study the dead time distortion, different slit widths were used (slits = 35 and 50 mm). The corresponding data rates were 7.861 and 12.416 events/frame, respectively. As shown in figure 10 (a, b), there exist distortions in early times in both slit widths, and they can be fitted by a simple exponential function. If the counting rate is higher, the distortion of the time spectrum in early times is more severe. These distortions can be removed by an appropriate correction. A non-paralyzable model is commonly used to describe the dead time behavior according to the analysis of G.F. Knoll [27]: $N = M/(1 - M\tau)$, where N is the true counting rate, M is the measured counting rate and τ is the system dead time. G.F. Knoll also provided a method of dead time measurement based on a short-lived radioisotope source, known as the decaying source method: $N = N_0 \exp(-\lambda t) + N_b$, where N_0 is the initial true

2019 JINST 14 T04004

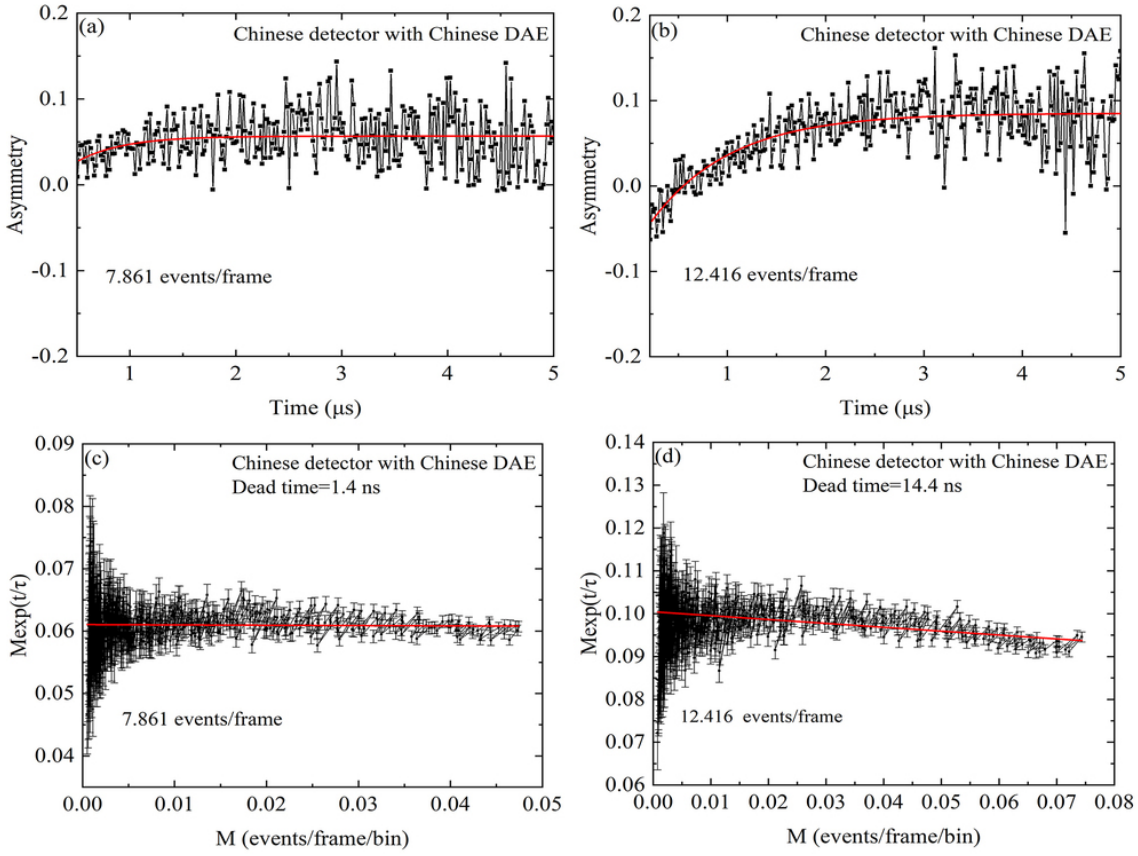

Figure 10. (a, b) Time-dependent plots of the muon asymmetry measured for our detection system at varying data rates. Fits to the data using a single exponential are shown in red curves. (c, d) Analysis of data measured for different data rates using the non-paralyzable deadtime model.

rate and λ is the particular isotope's decay constant, and N_b is the background. If the background is negligible, the equation can be simplified to $N = N_0 \exp(-\lambda t)$. By inserting this equation into the non-paralyzable model equation, the following relation can be obtained for the nonparalyzable model: $M \exp(\lambda t) = N_0 - N_0 M \tau$. The dead time τ will be given from the ratio of the slope to the intercept. As we know, a pulsed muon source can be regarded as a short-lived radioisotope source and there is almost no background in its μSR signals. Therefore, this dead time measurement method is applicable to our detection system. By plotting $M \exp(-t/\tau_\mu)$ against M (where M is the counting rate in each histogram bin recorded for each ISIS frame and τ_μ is the muon lifetime) [28], $M \exp(-t/\tau_\mu)$ against M should be fitted as a straight line. The dead time can be derived according to the slope and intercept of the line. Any departure of the data from this line suggests the model be invalid for the measurement system in use. Figure 10 (c, d) show the plot of $M \exp(-t/\tau_\mu)$ against M of different data rates. We can see the data of slit = 50 mm has departed from the line, it also means the dead time distortion is severe. The best dead time we achieved is 1.4 ns when the data rate is 7.861 events/frame. From the dead time test, we found that the dead time distortion is inevitable, but these distortions can be corrected. Our detection system works well when the data rate is below 10 events/frame. The dead time distortion can be eliminated by an appropriate data correction.

2019 JINST 14 T04004

4 Conclusions

We have completed the integrated design of 128-channel μSR spectrometer prototype of EMuS and the electronics including hardware and data acquisition software. According to the integrated design, one-channel μSR detector together with readout electronics was constructed and its performances were tested. Among these tests, the magnetic shield test and dead time test are the most important. A stable test method for the magnetic shielding capability has been developed by measuring the energy spectrum of ^{22}Na source. A magnetic field up to at least 30 Gauss can be eliminated by the proposed shielding. This satisfies the actual requirement of 8 Gauss. The beam test in ISIS muon facility was successful, demonstrating that the detection system can work well. The dead time of the prototype detector was measured with a dedicated setup and measured to be 1.4 ns. The construction and tests of this μSR detection system have an important guiding significance for completing the construction of the whole 128-channel μSR spectrometer prototype in the next step.

Acknowledgments

This work was supported by National Natural Science Foundation of China (Grant No. 11527811) and the key program of State Key Laboratory of Particle Detection and Electronics of China. We would like to thank Hamamatsu Photonics K.K. to provide the typical magnetic field characteristics of Hamamatsu R6427 in figure 5. We are grateful for the support of STFC ISIS Muon Group for our beam test, the technical support of Dr. Daniel Pooley and Stephen Cottrell, and the helpful discussions of Dr. Adrian Hillier, Isao Watanabe, James Lord, Nigel Rhodes, and Peter Baker.

References

[1] L. Nuccio, L. Schulz and A.J. Drew, *Muon spin spectroscopy: magnetism, soft matter and the bridge between the two*, *J. Phys.* **D 47** (2014) 473001.

[2] A. Yaouanc and P. Dalmas de Réotier, *Muon spin rotation, relaxation and resonance: applications to condensed matter,* Oxford University Press, Oxford, U.K. (2011).

[3] F.L. Pratt, P.J. Baker, S.J. Blundell, T. Lancaster, S. Ohira-Kawamura, C. Baines et al., *Magnetic and non-magnetic phases of a quantum spin liquid*, *Nature* **471** (2011) 612.

[4] T. Wu, H. Mayaffre, S. Krämer, M. Horvatić, C. Berthier, W. N. Hardy et al., *Magnetic-field-induced charge-stripe order in the high-temperature superconductor* $YBa_2Cu_3O_y$, *Nature* **477** (2011) 191.

[5] A.J. Drew, J. Hoppler, L. Schulz, F. L. Pratt, P. Desai, P. Shakya et al., *Direct measurement of the electronic spin diffusion length in a fully functional organic spin valve by low-energy muon spin rotation*, *Nat. Mater.* **8** (2008) 109.

[6] B. Chen, Z. Deng, W. Li, M. Gao, Q. Liu, C.Z. Gu et al., *New fluoride-arsenide diluted magnetic semiconductor (Ba,K)F(Zn,Mn)As with independent spin and charge doping*, *Sci. Rep.* **6** (2016) 36578.

[7] K. Nagamine, F. Pratt, S. Ohira, I. Watanabe, K. Ishida, S. Nakamura et al., *Intra- and inter-molecular electron transfer in cytochrome c and myoglobin observed by the muon spin relaxation method*, *Physica* **B 289–290** (2000) 631.

[8] *ISIS Muons webpage*, https://www.isis.stfc.ac.uk/Pages/Muons.aspx.

2019 JINST 14 T04004

[9] *PSI-LMU: Laboratory for Muon Spin Spectroscopy webpage*, https://www.psi.ch/lmu/.

[10] *J-PARC/MUSE webpage*, http://www.j-parc.jp/MatLife/en/index.html.

[11] *TRIUMF Centre for Molecular and Materials Science webpage*, http://cmms.triumf.ca/.

[12] J.E. Sonier, *Muon spin rotation/relaxation/resonance (μSR)*, http://www.chem.ubc.ca/sites/default/files/users/dgf/musrbrochure.pdf.

[13] J. Tang, X. Ni, X. Ma, H. Luo, Y. Bao, Y. Yuan et al., *EMuS muon facility and its application in the study of magnetism*, *Quantum Beam Sci.* **2** (2018) 23.

[14] E. Won, *A proposed muon facility in RAON/korea*, *JPS Conf. Proc.* **2** (2014) 010110.

[15] T.J. Williams and G.J. MacDougall, *Future muon source possibilities at the SNS*, Technical Report ORNL/TM-2017/165 (2017).

[16] RCNP-MuSIC webpage, http://www.rcnp.osaka-u.ac.jp/RCNPhome/music/.

[17] Z. Pan, X. Ni and B. Ye, *Conceptual design of MuSR spectrometer for EMuS using monte carlo simulation*, *JJAP Conf. Proc.* **7** (2018) 011303.

[18] M.Q. Zhuang et al., *The design of front-end electronics prototype for μSR spectrometer*, *Nucl. Electron. Detect. Technol.* **37** (2017) 463.

[19] F.S. Deng et al., *Design of a 32-channel TDC module based on single FPGA for μSR spectrometer prototype at CSNS*, to be published.

[20] O. Arnold et al., *Mantid — Data analysis and visualization package for neutron scattering and μSR experiments*, *Nucl. Instrum. Meth.* **A 764** (2014) 156 [arXiv:1407.5860].

[21] F.S. Deng et al., *Development of a Data Acquisition System for the μSR Spectrometer Prototype at the China Spallation Neutron Source*, submitted to *Nucl. Instrum. Meth.* **A**.

[22] *Hamamatsu webpage*, https://www.hamamatsu.com/.

[23] *Helmholtz coil webpage*, http://en.wikipedia.org/wiki/Helmholtz coil.

[24] P. Wang, Y. Zhang, X. Wang and Z. Xu, *Magnetic shield of PMT used in DAMPE electromagnetic calorimeter*, *Chin. Phys.* **C 38** (2014) 086002 [arXiv:1309.7638].

[25] *EMU spectrometer webpage*, https://www.isis.stfc.ac.uk/Pages/Emu.aspx.

[26] K. Nagamine, *Introductory muon science*, Cambridge University Press, Cambridge, U.K. (2007).

[27] G.F. Knoll, *Radiation detection and measurements*, John Willey and Sons, Inc., New York, NY, U.S.A. (2000).

[28] S.R. Giblin et al., *Optimising a Muon Spectrometer for Measurements at the ISIS Pulsed Muon Source*, *Nucl. Instrum. Meth.* **A 751** (2014) 70 [arXiv:1404.4542].

2019 JINST 14 T04004